

Unreal Robotics Lab: A High-Fidelity Robotics Simulator with Advanced Physics and Rendering

Jonathan Embley-Riches*, Jianwei Liu*, Simon Julier, and Dimitrios Kanoulas



Fig. 1: Examples of photorealistic rendering from our simulation framework, from left to right showing Unitree Go1 quadruped, Skydio X2 quadrocopter and Unitree B1-Z1 quadruped mobile manipulator in normal (top row) and adverse (bottom row) visual conditions.

Abstract—High-fidelity simulation is essential for robotics research, enabling safe and efficient testing of perception, control, and navigation algorithms. However, achieving both photorealistic rendering and accurate physics modeling remains a challenge. This paper presents a novel simulation framework—the Unreal Robotics Lab (URL) that integrates the Unreal Engine’s advanced rendering capabilities with MuJoCo’s high-precision physics simulation. Our approach enables realistic robotic perception while maintaining accurate physical interactions, facilitating benchmarking and dataset generation for vision-based robotics applications. The system supports complex environmental effects, such as smoke, fire, and water dynamics, which are critical for evaluating robotic performance under adverse conditions. We benchmark visual navigation and SLAM methods within our framework, demonstrating its utility for testing real-world robustness in controlled yet diverse scenarios. By bridging the gap between physics accuracy and photorealistic rendering, our framework provides a powerful tool for advancing robotics research and sim-to-real transfer.

I. INTRODUCTION

Simulation plays a crucial role in robotics research, enabling safe, efficient, and cost-effective development, testing, and validation of robotic systems before real-world deployment. High-fidelity simulation environments provide realistic perception and physics interactions, bridging the gap between simulation and reality. However, achieving both photorealism

The authors are with the Department of Computer Science, University College London, Gower Street, WC1E 6BT, London, UK. {jonathan.embley-riches.22, jianwei.liu.21, s.julier, d.kanoulas}@ucl.ac.uk

*equal contribution

This work was supported by the UKRI Future Leaders Fellowship [MR/V02533/1] (RoboHike) and the CDT for Foundational Artificial Intelligence [EP/S021566/1]. For the purpose of Open Access, the author has applied a CC BY public copyright license to any Author Accepted Manuscript version arising from this submission.

and accurate physics simultaneously remains a challenge due to computational constraints and the complexity of real-world dynamics [1].

This paper presents a novel simulation pipeline that combines the rendering capabilities of Unreal Engine [2] with the advanced physics simulation of MuJoCo [3] to create photorealistic environments for robotics applications. By integrating these two frameworks, our approach delivers high-quality simulation results suitable for tasks such as perception training, dataset generation, and benchmarking.

A key advantage of this pipeline is its ability to generate complex and dynamic environmental effects—such as smoke, fire, and water waves—which are crucial for training robots to handle diverse and unpredictable conditions. These effects enable the simulation of rare events that are difficult to capture in real-world datasets or reproduce in existing simulators. As a result, they can be used to benchmark vision-based policies under out-of-distribution conditions and generate training data for visual-based navigation.

We present a novel, open-source simulation framework—the Unreal Robotics Lab (URL) that integrates Unreal Engine for photorealistic rendering with MuJoCo for accurate physics simulation. Unlike existing simulators focused on specific domains (e.g., autonomous driving or aerial robotics) or embodied-ai for limited robots, our system is designed for **general-purpose robotic applications**, supporting quadrupeds, manipulators, UAVs, and more. Additionally, we incorporate **CoACD-based convex decomposition** [4] for improved non-convex object representation. Our key contributions are:

- **High-Fidelity Physics with Photorealistic Rendering:** Synchronization of MuJoCo’s physics with Unreal En-

gine’s advanced rendering (Lumen, Nanite, Niagara) enables realistic perception-based training and benchmarking.

- **Generalized Benchmarking for Diverse Conditions:** A structured benchmarking system evaluates robotic perception and control under rare conditions (e.g., smoke, fog, dynamic lighting, dynamic movement).
- **Scene Generation:** A GPT-based module automates diverse environment creation, reducing manual setup and enabling adaptive scene variations.
- **Comprehensive Sensor and Control Framework:** Built-in support for cameras, IMUs, force sensors, and controllers for various robot types, with full Robot Operating System (ROS) compatibility.
- **Open-Source and Extensible:** The system will be released as open-source, supporting modular extensions for new controllers, planners, and robotic platforms.

The subsequent sections are structured as follows. Sec. II provides an overview of the relevant literature, discussing previous works in the field, while Sec. III outlines the proposed method in detail. Sec. IV presents the experimental setup, including both simulation and real robot experiments. Finally, in Sec. V, we present the conclusions and discuss future

II. RELATED WORK

Robotic simulation has advanced significantly in recent years, with various frameworks addressing key challenges such as physics accuracy, photorealistic rendering, and real-time performance. This section reviews related work in three main areas: robotics-focused simulation platforms, comparisons of physics engines, and benchmarking SLAM and navigation under adverse visual conditions.

Several other game engines and simulation platforms offer photorealistic rendering [5], [6], [7], but Unreal Engine provides distinct advantages through Lumen global illumination and Nanite virtualized geometry. Unlike other simulators that rely on hardware-intensive ray tracing, Lumen [8] enables real-time global illumination and reflections without requiring precomputed lighting, making it well-suited for dynamic environments where lighting conditions change.

Furthermore, Nanite’s automatic level of detail (LOD) [9] system allows highly detailed assets with millions of triangles to be rendered efficiently, without affecting performance. This is particularly beneficial for large-scale or high-fidelity indoor environments where maintaining real-time performance is critical. Beyond rendering, Unreal Engine offers a flexible and extensible ecosystem, supporting third-party plugins, visual scripting, AI-driven NPCs, and cross-platform deployment, making it highly adaptable for a variety of robotic simulation tasks. These features ensure that simulations can achieve both high physical accuracy and photorealistic perception, making them an ideal choice for vision-based robotics research.

A. Robotics-Focused Simulation Platforms

Robotic simulation has made considerable progress, with numerous frameworks addressing challenges in physics ac-

curacy, rendering quality, and real-time performance. This section reviews related work in three primary areas: robotics simulation platforms, comparisons of physics engines, and benchmarking of SLAM and navigation under adverse visual conditions.

Several simulation platforms have been developed for robotic perception, control, and reinforcement learning, each with different trade-offs in realism and efficiency. Gazebo [10] is a widely-used open-source simulator that supports multiple physics engines; ODE [10], Simbody [11], (Py)Bullet [12], and DART [13], although its rendering capabilities lag behind modern game-engine-based simulators. MuJoCo [3] excels in efficient and accurate physics modeling for robotic control but lacks built-in photorealistic rendering. GPU-accelerated platforms such as Isaac Orbit [5] and Isaac Gym [14] enable large-scale reinforcement learning, prioritizing speed over advanced rendering. Intel SPEAR [15] provides photorealistic indoor environments suitable for embodied AI research. CARLA [7] and AirSim [16] leverage Unreal Engine for photorealistic urban and aerial simulations, with a primary focus on autonomous driving and drone applications. CARLA, in particular, emphasizes high-level decision-making, such as traffic light interactions and multi-agent traffic flow, rather than fine-grained vehicle dynamics like tire skidding. However, both simulators remain largely domain-specific, limiting their utility for broader robotics applications beyond driving and aerial scenarios. RoboSuite [17] and RoboCasa [18] emphasize robotic manipulation using MuJoCo for precise physics but offer limited environmental complexity. MetaUrban [19] simulates realistic urban environments with dynamic traffic, beneficial for multi-agent interactions.

Although most simulators prioritize either physics accuracy or visual realism, few achieve both. Our approach bridges this gap by integrating MuJoCo for precise physics with Unreal Engine for state-of-the-art rendering, creating a high-fidelity simulation pipeline for diverse robotic applications.

B. Physics Engines for Robotics Simulation

Physics engines are essential for realistic robotic simulation, particularly for modeling contact, soft-body dynamics, and fluid interactions. Various engines have been evaluated in terms of accuracy, efficiency, and scalability, with notable differences in their suitability for robotics [20]. MuJoCo [3] excels in soft-contact modeling, accuracy, and stability, making it ideal for complex robotic tasks such as grasping and locomotion. However, it lacks built-in high-fidelity rendering. ODE (Open Dynamics Engine) [10], commonly used in Gazebo, faces stability issues in high-DOF tasks and requires extensive parameter tuning. Bullet [12] is popular for reinforcement learning and manipulation, but its precision lags behind MuJoCo.

Unreal Engine’s Chaos and Havok [21] are optimized for game physics and real-time effects, excelling in destruction, fluid, and particle-based simulations. However, they are not designed for robotic applications that need soft-

contact modeling or high-precision joint dynamics. NVIDIA PhysX [22] offers GPU-accelerated simulation suitable for fast reinforcement learning, but its omission of Coriolis forces makes it unsuitable for high-accuracy control.

Our approach combines MuJoCo’s precise physics with Unreal Engine’s advanced rendering, achieving both photorealism and accurate simulation for robotic applications.

C. Benchmarking SLAM and Navigation Under Adverse Visual Conditions

Evaluating SLAM and navigation algorithms in diverse environments is challenging, as many existing datasets capture structured scenarios under ideal conditions, making it difficult to test performance under adverse effects such as smoke, fog or dynamic lighting.

Envodat [23] provides a dataset tailored for challenging conditions, but real-world data collection remains limited in scale and diversity. Our simulation pipeline fills this gap by synthetically generating rare-event scenarios, enabling benchmarking and training of vision-based navigation policies in controlled, repeatable settings.

Current simulation platforms often emphasize either high-precision physics (e.g., MuJoCo, Isaac Gym) or photorealistic rendering (e.g., Unreal-based simulators such as Carla and AirSim). A recent simulator, SPEAR [15], integrates MuJoCo with Unreal Engine but primarily focuses on providing a Python-based OpenAI Gym environment, pre-built scenes, limited robot support, and task-specific benchmarks. In contrast, our approach integrates MuJoCo’s precise physics with Unreal Engine’s advanced rendering in a flexible and generalized simulation environment. Our framework allows users to freely configure robots and tasks, and utilizes ROS to treat simulated interactions as closely as possible to real-world scenarios. Furthermore, by leveraging Unreal’s Niagara Particle and Fluid effects, we enable simulation of adverse environmental conditions such as smoke, fire, and water waves, extending traditional benchmarking capabilities and providing robust tools for evaluating robotic perception and navigation under challenging scenarios.

III. SIMULATOR SETUP

A. Overview

Our simulator (URL) integrates MuJoCo and Unreal Engine to provide a comprehensive simulation environment that closely mimics real-world interactions. Robots can be effortlessly integrated by adding corresponding MuJoCo XML descriptions and associated Unreal Engine assets. The system supports standard robot configurations and sensors, including cameras, IMUs, and force sensors, ensuring wide compatibility. The overall system can be seen in Figure 4. The system is comprised of both External components and the internal simulator. The system has a SimManager that is modular and manages submodules comprised of a Benchmark, Replay, and SceneGen modules. It manages all references to the UE data and is developed as a plugin for UE that can be added to any project.

For communication, our simulator leverages ROS to enable seamless interaction with existing robotics frameworks. Furthermore, faster custom communication methods are being explored through ZeroMQ [24] for improved real-time performance. We treat the simulation environment as a surrogate *real-world*, facilitating the testing and validation of robotic behaviors and perception systems in realistic scenarios.

B. Physics Manager

Our system integrates MuJoCo and CoACD [4] within the Unreal Engine (UE) for accurate physics simulation and mesh decomposition. These systems are currently compiled into the UE project, and extend a custom interface. To represent objects in the scene, we introduce an intermediate representation, termed *PhysicsObject*, which encapsulates both geometric and state information. This allows us to efficiently manage and transform scene elements between UE and MuJoCo while ensuring that transformations and dynamic interactions are correctly synchronized.

Objects within the scene are categorized into predefined types. Specifically, assets are tagged under one of the following categories: EP_STATIC, EP_STATIC_COMPLEX, EP_DYNAMIC, EP_DYNAMIC_COMPLEX, and EP_PRIMITIVE_(TYPE). Static objects remain unchanged throughout the simulation, whereas dynamic objects are actively tracked, with their transformations updated asynchronously within UE. The distinction between simple and complex dynamic objects determines whether the object undergoes convex decomposition by CoACD. CoACD decomposes meshes into a series of convex hulls, whereas the regular mujoco compile will generate only one convex hull per object. This allows CoACD to represent non-convex geometry and is recommended by MuJoCo [20]. This classification is recorded within the corresponding *PhysicsObject* to guide further processing. Once asset classification is complete, mesh-based assets are exported as OBJ files, ensuring compatibility with MuJoCo. Additionally, if landscapes are present in the scene, they are scanned and converted into height-fields to be used within the simulation. This process uses a custom collision channel on the landscape, then, utilizing an autogenerated bounding box, we perform multithreaded raycasts to determine the heights to use. This bounding-box limits the raycasts to within this area only at a predefined resolution. This prevents the whole landscape from being scanned. Figure 3



(a) Unreal Engine Landscape (b) MuJoCo HeightField

Fig. 3: Unreal Engine Landscape conversion to MuJoCo HeightField.

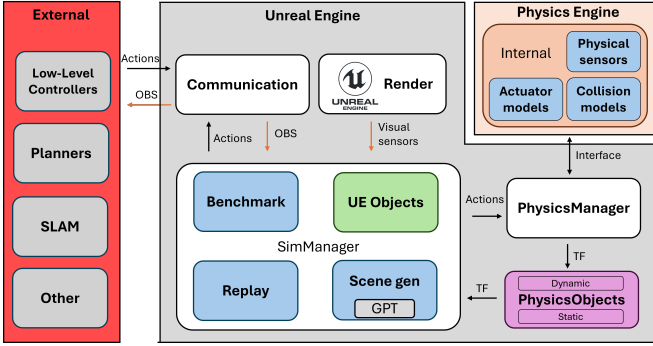


Fig. 4: Unreal - Mujoco Simulator system diagram

demonstrates the output of this process. This method was chosen because landscapes can be very large, and the user may not be interested in converting the entire landscape for physics. It also has the added benefit of being able to model small clutter and decorations in the heightfield itself. This process enables the seamless reconstruction of large-scale terrains within MuJoCo, preserving critical environmental features necessary for accurate physics interactions.

Following asset processing, an XML scene description is automatically generated to initialize MuJoCo. This XML encapsulates all relevant object data, including mesh file references, physics properties, and hierarchical relationships. Special attention is paid to robotic assets that are detected within the MuJoCo environment and mapped back to their corresponding UE entities. During this process, cameras and sensors specified in the XML are instantiated within UE to ensure consistency across both environments. Sensor elements are represented as *sites* within MuJoCo, allowing for precise placement and interaction within the physics simulation.

The physics simulation operates asynchronously, running within a separate execution thread to maximize performance. Transformation updates are also managed in a dedicated asynchronous thread within UE to maintain real-time synchronization with MuJoCo. External forces applied within MuJoCo can be propagated to UE entities, allowing for bidirectional interaction between the simulation and the rendered environment. UE physics can still be used for objects not managed by MuJoCo.

To improve computational efficiency, assets that remain unchanged between simulation runs are cached, preventing unnecessary recomputation and redundant file exports. This caching mechanism ensures that static elements do not incur additional processing overhead, allowing the system to focus on dynamic entities that require continuous state updates. The final XML scene description, along with the automatically generated mesh assets, enables direct execution within MuJoCo as a standalone simulation. A supporting script is provided to facilitate this process, allowing the same environment to be used independently of UE when required.

C. Benchmark System

The benchmarking system automates the recording and management of evaluation metrics throughout the simulation.



Fig. 5: Example of room generated using the experimental Scene Generation system leveraging GPT API.

At its core, it consists of a *MetricManager* and a *BaseMetric* class, providing a structured and extensible framework to track performance indicators.

The *BaseMetric* class defines a fundamental interface for all metrics, encapsulating a two-dimensional float array that serves as a storage mechanism for time-series data. This class provides essential methods, including initialization, resetting, and exporting data to CSV format. These methods ensure that each metric implementation adheres to a consistent lifecycle, simplifying the process of integrating new metrics into the system. Derived metrics can override these base methods to implement domain-specific logic while still benefiting from the structured data storage and export mechanisms.

The *MetricManager* is responsible for the automatic discovery and registration of all metric implementations. It dynamically populates a list of available metrics by scanning for corresponding class definitions, allowing modular and scalable metric tracking. Users can enable or disable specific metrics through a dedicated user interface, ensuring flexibility in selecting relevant performance indicators for a given experiment.

By default, the system tracks core metrics, including: *DistanceToGoal*, which tracks the remaining distance from an entity to a predefined target location; *Collisions*, which records contact events with obstacles or other entities; *TimeToGoal*, which measures the time required to reach the destination; and *GlobalPose*, which logs the absolute position and orientation of an entity over time.

All metrics are recorded at discrete intervals and automatically saved as CSV files within designated experiment folders, ensuring organized and accessible results. The system also features grace periods (delaying data recording for n seconds) and timeouts (terminating recordings after n seconds), improving efficiency and reproducibility across simulation runs.

D. Scene Generation

Our simulator features an experimental scene generation module designed primarily for indoor environments, leveraging OpenAI's ChatGPT [25] API. When an instance of the *ASceneGenerator* Actor is present and assigned a *RoomType*, the system automatically generates object placements based on the specified scene type (Fig. 5). The module queries ChatGPT with a structured prompt containing a list of available assets and receives a JSON-formatted response specifying object positions. These placements are then parsed, and

the corresponding assets are instantiated in the environment.

To ensure spatial coherence, the system detects overlapping objects using Unreal Engine’s physics system. If overlaps occur, an iterative refinement loop provides feedback to ChatGPT for updated placement recommendations, continuing until all collisions are resolved or a predefined iteration limit is reached. This method enables efficient, collision-free scene generation, producing diverse and structured environments suitable for robotic experimentation.

E. Replay

Our system features an automated recording and replay mechanism for sensor and body pose data, enabling efficient data collection and experimentation. It uses custom structs to track only essential information –pose data, sensor readings, and timestamps– storing them in a queue for minimal overhead and precise sequence reproduction. Data streams are managed through separate JSON files, all of which can be dynamically saved and loaded at runtime. By publishing replayed data on the same ROS topics as live data, the system integrates seamlessly with existing pipelines. This allows researchers to collect data once and replay it in visually modified environments, supporting domain adaptation, robustness testing, and dataset augmentation for machine learning and benchmarking.

F. Extended Features

Our system leverages Unreal Engine’s advanced rendering and simulation capabilities, surpassing traditional robotics simulators like MuJoCo [3], Gazebo [10], and Isaac Sim [5]. Key features include real-time global illumination (Lumen), high-detail mesh rendering (Nanite), and physically based reflections, which enhance perception-based robotics research. Procedural animations, NavMesh navigation, and built-in environmental tools enable efficient creation of dynamic simulations, while the Niagara particle system facilitates testing under adverse visual conditions (e.g., smoke, fog). Additionally, packaged standalone deployments improve reproducibility and scalability, addressing limitations of conventional simulators.

G. Example Deployment of Robots, Controllers, and Visual Planners

The system provides a unified framework where robots, controllers, and planners operate as in real-world deployments. All components communicate through ROS, ensuring seamless integration with external systems.

1) *Example Robot Integrations*: The framework supports quadrupeds, quadruped mobile manipulators, UAVs, and robotic manipulators, enabling diverse experimental setups for locomotion, aerial navigation, and manipulation.

2) *Controllers*: The system includes joint controllers based on position and torque, as well as more advanced controllers such as Walk-These-Ways [26] and VBC [27]. UAVs use a PID-based controller, whereas manipulators rely on inverse kinematics (IK) methods such as Mink [28]. Since controllers operate within the ROS ecosystem, new control strategies can be easily integrated.

3) *Planners*: Motion planning is handled using learning-based and optimization-based planners such as ViNT [29], GNM [30], and NoMAD [31]. The ROS-based architecture of the framework ensures compatibility with additional external planners.

4) *Visual SLAM*: The system includes visual SLAM techniques such as OrbSLAM2 [32], OrbSLAM3 [33], and MAS3R-SLAM [34], enabling real-time localization and mapping. These methods integrate directly into the framework, enabling realistic perception and mapping in simulated environments.

IV. EXPERIMENTS

A. Simulation and Real-World Comparision

To evaluate the alignment between simulated and real-world visual inputs for image encoders, we employ Grad-CAM, EigenCAM, cosine similarity and KL Divergence. These methods assess both spatial attention and feature distribution similarity.

Grad-CAM computes the gradient of the class score y^c with respect to feature map activations:

$$\alpha_k^c = \frac{1}{Z} \sum_i \sum_j \frac{\partial y^c}{\partial A_{ij}^k}, \quad L^c = \text{ReLU} \left(\sum_k \alpha_k^c A^k \right) \quad (1)$$

EigenCAM generates class-agnostic saliency maps via principal component analysis (PCA):

$$C = \frac{1}{Z} \sum_{i,j} (A_{ij}^k - \mu)(A_{ij}^k - \mu)^T, \quad L_{\text{EigenCAM}} = v_1 A^k \quad (2)$$

where μ is the mean activation and v_1 is the first principal component.

Cosine Similarity measures feature alignment between real and simulated embeddings:

$$S_{\text{cosine}}(P, Q) = \frac{P \cdot Q}{\|P\| \|Q\|} \quad (3)$$

where P and Q are feature vectors. Higher values indicate stronger similarity.

KL Divergence quantifies distribution differences:

$$D_{\text{KL}}(P\|Q) = \sum_i P(i) \log \frac{P(i)}{Q(i)} \quad (4)$$

Lower values indicate closer alignment.

To compare models trained on real-world data, we use CLIP [35] and the EfficientNet-B0 [36] visual encoder used in ViNT [29]. We first capture an image from the real world and recreate it within our simulator. Then both images are processed using Grad-CAM and Eigen-Cam to generate attention heatmaps, as shown in Figure 6.

In both cases, the models primarily attend to the traffic cone in the center of the hallway as well as the end of the corridor, suggesting that the most salient features are preserved between the real and simulated environments. This alignment indicates that the models are focusing on the same high-level structures regardless of domain, reinforcing the realism of

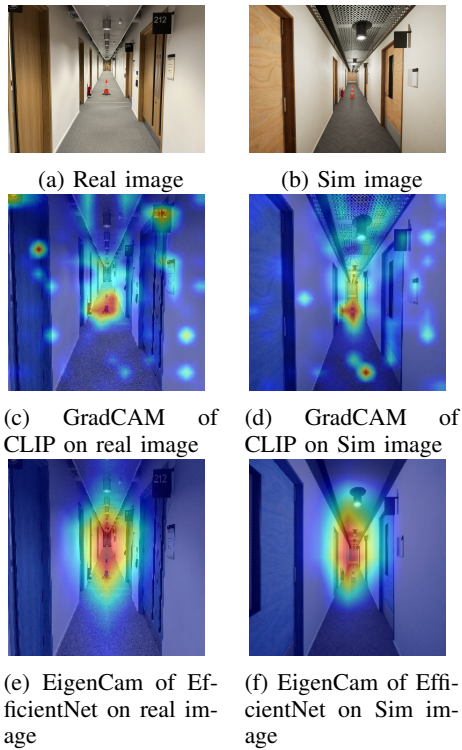


Fig. 6: Comparison of real-world (left) and simulated (right) images, along with their corresponding Grad-CAM (CLIP) and EigenCAM (EfficientNet-B0) heatmaps. The highlighted class label is "cone".

the simulated scene in terms of feature representation. The similarity in attention patterns also suggests that key objects remain distinguishable across domains, which is critical for transfer learning and sim-to-real applications.

To further quantify similarity, we compute KL divergence (0.4679) and cosine similarity (0.7157) between real and simulated feature distributions. Higher cosine similarity and lower KL divergence suggest closer alignment. While we did not aim to replicate real-world scenes with identical assets, opting instead for a simulation that remains visually representative of real conditions. Although the assets in our simulation differ from those in the real environment, our findings, together with GradCAM and EigenCAM comparisons, indicate that the simulation is visually representative enough for our evaluation purposes.

B. Visual Navigation and SLAM Benchmarking

we benchmark standard methods to demonstrate simulator realism. We evaluated visual navigation (Experiment 1) with GNM [30] and ViNT [29], and visual SLAM (Experiment 2) with OrbSLAM2 [32], OrbSLAM3 [33], and MASt3R-SLAM [34]. Each method was run 5 times per condition, averaging results across trials. Both experiments used the Unitree Go1 quadruped with its onboard camera and the Walk-These-Ways low-level controller for realistic deployment.

The benchmarks were conducted in two distinct environments—warehouse and residential house—under three

Env	Adversity	Method	Success rate↑	Collisions↓	Time to Goal↓	Goal Dist↓	Weighted SC↑
House	Major	GNM	0.2	13	0	7.01	0.0154
		ViNT	0	9.2	0	8.41	0
	Minor	GNM	1	1.2	71.59	1.99	0.5333
Warehouse	None	GNM	1	1.8	147.86	1.99	0.3667
		ViNT	1	0.8	141.35	2.00	0.7333
	Major	GNM	0	12.8	0	8.33	0
Warehouse		ViNT	0	6.4	0	7.96	0
	Minor	GNM	0.4	4	107.62	4.69	0.1067
		ViNT	0.2	6.6	54.91	6.61	0.0250
None	GNM	0.8	3.4	102.86	2.53	0.1889	
	ViNT	0.8	4.4	90.14	2.59	0.3667	

TABLE I: Performance of different Visual navigation methods under various environments and varying adverse effects.

adversity levels: none, minor and major, classified by human judgment. UE’s Niagara system simulated environmental effects (smoke, rain, pollution, snow), while dynamic lighting and NPC movements were added for major adversity. Figure 1 shows example environments and Figure 7 shows examples of adversity levels.

1) *Experiment 1: Visual Navigation*: For visual navigation benchmarking, the robot was initialized at identical starting locations across environments and adversity levels. Each method had a fixed duration to reach the goal using a pre-built image-based topological map. The warehouse and residential house were used for this experiment. Methods were not fine-tuned, relying on a simplified topological map approach from the authors’ original repository [31], which may limit performance [37].

Success Weighted by Collision (SC). Following [38], we adopt the SC metric:

$$SC = \frac{1}{N} \sum_{i=1}^N S_i \frac{1}{1 + c_i}, \quad (5)$$

where S_i is the success indicator for episode i , c_i is the number of collisions, and N is the total episodes. Higher SC values indicate fewer collisions in successful runs, while lower values reflect frequent or severe collisions. Alongside SC, we measure success rate, total collisions, time to goal, and goal distance.

Table I presents the results, including Weighted SC to factor in collision penalties. State-of-the-art methods perform well under normal conditions, with ViNT generally outperforming GNM. Under minor adversity, GNM maintains a higher success rate but takes longer, while ViNT completes



Fig. 7: Examples of the different adversity levels for the House Environment.

Env	Adver.	OrbSLAM2 Mono			OrbSLAM3 Mono			MASt3R-SLAM		
		ATE↓	Scaled ATE↓	Cover- age↑	ATE↓	Scaled ATE↓	Cover- age↑	ATE↓	Scaled ATE↓	Cover- age↑
Warehouse	None	4.23	6.61	0.639	5.29	7.72	0.685	0.324	0.322	1.01
	Minor	5.33	10.1	0.527	5.21	8.80	0.592	1.55	1.77	0.872
	Major	2.96	20.2	0.147	4.29	5.87	0.731	0.252	0.417	0.605
House	None	3.49	4.64	0.752	1.69	1.17	1.45	0.274	0.326	0.840
	Minor	0.513	1.23	0.415	0.547	1.81	0.302	0.257	0.300	0.855
	Major	0.475	2.53	0.188	2.70	11.6	0.233	0.275	0.284	0.966

TABLE II: Performance of Different VSLAM Methods under Varying Visual Effects.

faster when successful. However, performance declines as environmental adversity increases (e.g., obstacles, smoke, rain), with both methods experiencing more collisions, longer times to goal, and lower SC. In severe adversity, neither method succeeds in the Warehouse, leading to zero SC. This suggests that these models struggle in extreme conditions due to limited training data, highlighting the need for training in diverse high-adversity conditions, which can be generated more effectively in simulation. The ability to create controlled but realistic adverse scenarios in a simulated environment provides a path to improve robustness in real-world deployments.

2) Experiment 2: Visual SLAM: This experiment used our replay system, where a teleoperated robot followed predefined trajectories optimized for SLAM. Initial runs recorded robot poses and sensor data, which were later replayed with identical conditions but varying visual effects. Each SLAM method was then evaluated, and performance metrics were computed.

Absolute Trajectory Error (ATE) measures the global accuracy of an estimated trajectory by computing the RMSE between estimated positions $\hat{\mathbf{p}}_i$ and ground truth positions \mathbf{p}_i :

$$\text{ATE} = \sqrt{\frac{1}{n} \sum_{i=1}^n (\mathbf{p}_i - \hat{\mathbf{p}}_i)^2} \quad (6)$$

Coverage measures the ratio of the estimated trajectory length to the ground truth:

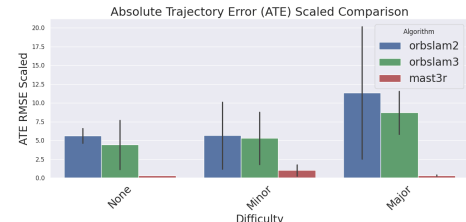
$$\text{Coverage} = \frac{\sum_{i=1}^{n-1} \|\mathbf{p}_{i+1} - \mathbf{p}_i\|}{\sum_{i=1}^{n-1} \|\hat{\mathbf{p}}_{i+1} - \hat{\mathbf{p}}_i\|} \quad (7)$$

note that since monocular SLAM estimates trajectories with arbitrary scale, Umeyama’s method [39] is applied for scale and pose correction before computing coverage. Poor tracking or alignment can result in coverage exceeding 100%.

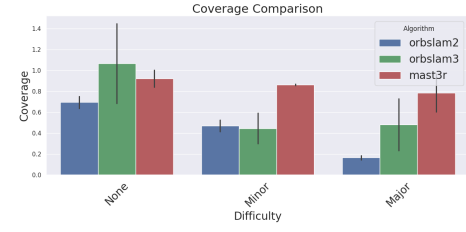
Scaled ATE adjusts ATE for localization failures:

$$\text{Scaled ATE} = \frac{\text{ATE}}{\text{Coverage}} \quad (8)$$

From Table II and Fig. 8, Visual SLAM performance degrades with increasing visual adversity, highlighting sensitivity to challenging conditions. OrbSLAM2 struggles the most, with sharp declines in coverage and increased ATE, particularly in the warehouse environment. OrbSLAM3 performs well in clean conditions but deteriorates significantly



(a) Scaled ATE



(b) Coverage

Fig. 8: comparision of different Visual SLAM algorithms under different visual effects

under adversity, suggesting reduced robustness to occlusions, lighting changes, and dynamic elements. MASt3R-SLAM maintains the lowest ATE and highest coverage across conditions, demonstrating superior resilience to visual disturbances. Under severe visual adversity, all methods experience increased ATE and reduced coverage, highlighting the inherent challenges of maintaining reliable SLAM performance in dynamic or visually degraded environments. These replay-based evaluations provide a controlled, repeatable framework for assessing SLAM robustness across different levels of adversity, reinforcing the need for training and evaluation in diverse, high-adversity conditions to enhance real-world deployment reliability.

V. CONCLUSION

This paper presents a high-fidelity robotics simulation framework that integrates advanced photorealistic rendering with precise physics modeling to support vision-based robotics research and benchmarking. By leveraging Unreal Engine’s rendering capabilities and MuJoCo’s accurate physics, our system enables evaluation of robotic navigation and SLAM methods under diverse and adverse environmental conditions. Experimental results confirm that our simulator provides a robust testbed for evaluating real-world robustness in controlled, repeatable scenarios.

Despite its strengths, the system has certain limitations, including the absence of direct reinforcement learning (RL) support, lack of deformable terrain simulation, limited scene generation capabilities, and a focus on general robotics rather than autonomous vehicles or high-precision drone simulations.

Future Work. To address these limitations and further enhance our simulator, we plan to further enhance the MuJoCo integration, allowing the simulator to communicate with a standalone MuJoCo process and run RL environments (MuJoCo Playground [40]), generate synthetic datasets

to enhance vision-based model training, expand automated scene generation, and enable imitation learning via VR-based teleoperation.

Overall, our platform serves as a robust foundation for benchmarking and data generation, bridging the gap between simulation and real-world robotics deployment.

REFERENCES

- [1] A. Szot, A. Clegg, E. Undersander, E. Wijmans, Y. Zhao, J. Turner, N. Maestre, M. Mukadam, D. S. Chaplot, O. Maksymets, *et al.*, “Habitat 2.0: Training home assistants to rearrange their habitat,” *Advances in neural information processing systems*, vol. 34, pp. 251–266, 2021.
- [2] Epic Games, “Unreal Engine.” [Online]. Available: <https://www.unrealengine.com>
- [3] E. Todorov, T. Erez, and Y. Tassa, “MuJoCo: A physics engine for model-based control,” in *2012 IEEE/RSJ international conference on intelligent robots and systems*. IEEE, 2012, pp. 5026–5033.
- [4] X. Wei, M. Liu, Z. Ling, and H. Su, “Approximate convex decomposition for 3d meshes with collision-aware concavity and tree search,” *ACM Transactions on Graphics (TOG)*, vol. 41, no. 4, pp. 1–18, 2022.
- [5] M. Mittal, C. Yu, Q. Yu, J. Liu, N. Rudin, D. Hoeller, J. L. Yuan, R. Singh, Y. Guo, H. Mazhar, *et al.*, “Orbit: A unified simulation framework for interactive robot learning environments,” *IEEE Robotics and Automation Letters*, vol. 8, no. 6, pp. 3740–3747, 2023.
- [6] X. Puig, E. Undersander, A. Szot, M. D. Cote, T.-Y. Yang, R. Partsey, R. Desai, A. W. Clegg, M. Hlavac, S. Y. Min, *et al.*, “Habitat 3.0: A co-habitat for humans, avatars and robots,” *arXiv preprint arXiv:2310.13724*, 2023.
- [7] A. Dosovitskiy, G. Ros, F. Codevilla, A. Lopez, and V. Koltun, “CARLA: An open urban driving simulator,” in *Conference on robot learning*. PMLR, 2017, pp. 1–16.
- [8] E. Games, “Lumen: Global illumination and reflections in unreal engine,” Epic Games Documentation, 2025, accessed: 2025-03-01. [Online]. Available: <https://dev.epicgames.com/documentation/en-us/unreal-engine/lumen-global-illumination-and-reflections-in-unreal-engine>
- [9] ———, “Nanite: Virtualized geometry in unreal engine,” Epic Games Documentation, 2025, accessed: 2025-03-01. [Online]. Available: <https://dev.epicgames.com/documentation/en-us/unreal-engine/nanite-virtualized-geometry-in-unreal-engine>
- [10] N. Koenig and A. Howard, “Design and use paradigms for gazebo, an open-source multi-robot simulator,” in *2004 IEEE/RSJ international conference on intelligent robots and systems (IROS)(IEEE Cat. No. 04CH37566)*, vol. 3. IEEE, 2004, pp. 2149–2154.
- [11] M. A. Sherman, A. Seth, and S. L. Delp, “Simbody: multibody dynamics for biomedical research,” *Procedia Iutam*, vol. 2, pp. 241–261, 2011.
- [12] E. Coumans and Y. Bai, “Pybullet, a python module for physics simulation for games, robotics and machine learning,” 2016.
- [13] J. Lee, M. X. Grey, S. Ha, T. Kunz, S. Jain, Y. Ye, S. S. Srinivasa, M. Stilman, and C. Karen Liu, “Dart: Dynamic animation and robotics toolkit,” *The Journal of Open Source Software*, vol. 3, no. 22, p. 500, 2018.
- [14] V. Makoviychuk, L. Wawrzyniak, Y. Guo, M. Lu, K. Storey, M. Macklin, D. Hoeller, N. Rudin, A. Allshire, A. Handa, *et al.*, “Isaac gym: High performance gpu-based physics simulation for robot learning,” *arXiv preprint arXiv:2108.10470*, 2021.
- [15] M. Roberts, R. Prakash, R. Wang, Q. Leboutet, S. R. Richter, S. Leutenegger, R. Tang, M. Müller, G. Ros, and V. Koltun, “SPEAR: A simulator for photorealistic embodied ai research,” <http://github.com/spear-sim/spear>.
- [16] S. Shah, D. Dey, C. Lovett, and A. Kapoor, “Airsim: High-fidelity visual and physical simulation for autonomous vehicles,” in *Field and Service Robotics: Results of the 11th International Conference*. Springer, 2018, pp. 621–635.
- [17] Y. Zhu, J. Wong, A. Mandlekar, R. Martín-Martín, A. Joshi, K. Lin, A. Maddukuri, S. Nasiriany, and Y. Zhu, “robosuite: A Modular Simulation Framework and Benchmark for Robot Learning,” in *arXiv preprint arXiv:2009.12293*, 2020.
- [18] S. Nasiriany, A. Maddukuri, L. Zhang, A. Parikh, A. Lo, A. Joshi, A. Mandlekar, and Y. Zhu, “RoboCasa: Large-Scale Simulation of Everyday Tasks for Generalist Robots,” in *Robotics: Science and Systems*, 2024.
- [19] W. Wu, H. He, J. He, Y. Wang, C. Duan, Z. Liu, Q. Li, and B. Zhou, “MetaUrban: An Embodied AI Simulation Platform for Urban Micromobility,” *arXiv preprint arXiv:2407.08725*, 2024.
- [20] T. Erez, Y. Tassa, and E. Todorov, “Simulation tools for model-based robotics: Comparison of bullet, havok, mujoco, ode and physx,” in *2015 IEEE international conference on robotics and automation (ICRA)*. IEEE, 2015, pp. 4397–4404.
- [21] Havok. “Havok Physics.” [Online]. Available: <https://www.havok.com/>
- [22] NVIDIA, “NVIDIA PhysX.” [Online]. Available: <https://developer.nvidia.com/physx-sdk>
- [23] L. Nwankwo, B. Ellensohn, V. Dave, P. Hofer, J. Forstner, M. Villeneuve, R. Galler, and E. Rueckert, “Envodat: A large-scale multisensory dataset for robotic spatial awareness and semantic reasoning in heterogeneous environments,” *arXiv preprint arXiv:2410.22200*, 2024.
- [24] F. Akgul, *ZeromQ*. Packt Publishing, 2013.
- [25] OpenAI, “Chatgpt,” 2025, accessed: 2025-02-28. [Online]. Available: <https://chat.openai.com/>
- [26] G. B. Margolis and P. Agrawal, “Walk these ways: Tuning robot control for generalization with multiplicity of behavior,” in *Conference on Robot Learning*. PMLR, 2023, pp. 22–31.
- [27] M. Liu, Z. Chen, X. Cheng, Y. Ji, R. Qiu, R. Yang, and X. Wang, “Visual Whole-Body Control for Legged Loco-Manipulation,” *The 8th Conference on Robot Learning*, 2024.
- [28] K. Zakka, “Mink: Python inverse kinematics based on MuJoCo,” July 2024. [Online]. Available: <https://github.com/kevinzakka/mink>
- [29] D. Shah, A. Sridhar, N. Dashora, K. Stachowicz, K. Black, N. Hirose, and S. Levine, “ViNT: A Foundation Model for Visual Navigation,” in *Conference on Robot Learning*. PMLR, 2023, pp. 711–733.
- [30] D. Shah, A. Sridhar, A. Bhorkar, N. Hirose, and S. Levine, “Gnm: A general navigation model to drive any robot,” in *2023 IEEE International Conference on Robotics and Automation (ICRA)*. IEEE, 2023, pp. 7226–7233.
- [31] A. Sridhar, D. Shah, C. Glossop, and S. Levine, “Nomad: Goal masked diffusion policies for navigation and exploration,” in *2024 IEEE International Conference on Robotics and Automation (ICRA)*. IEEE, 2024, pp. 63–70.
- [32] R. Mur-Artal and J. D. Tardós, “ORB-SLAM2: an open-source SLAM system for monocular, stereo and RGB-D cameras,” *IEEE Transactions on Robotics*, vol. 33, no. 5, pp. 1255–1262, 2017.
- [33] C. Campos, R. Elvira, J. J. G. Rodríguez, J. M. Montiel, and J. D. Tardós, “Orb-slam3: An accurate open-source library for visual, visual-inertial, and multimap slam,” *IEEE Transactions on Robotics*, vol. 37, no. 6, pp. 1874–1890, 2021.
- [34] R. Murai, E. Dexheimer, and A. J. Davison, “Mast3r-slam: Real-time dense slam with 3d reconstruction priors,” *arXiv preprint arXiv:2412.12392*, 2024.
- [35] A. Radford, J. W. Kim, C. Hallacy, A. Ramesh, G. Goh, S. Agarwal, G. Sastry, A. Askell, P. Mishkin, J. Clark, *et al.*, “Learning transferable visual models from natural language supervision,” in *International conference on machine learning*. PMLR, 2021, pp. 8748–8763.
- [36] M. Tan and Q. Le, “Efficientnet: Rethinking model scaling for convolutional neural networks,” in *International conference on machine learning*. PMLR, 2019, pp. 6105–6114.
- [37] R. Dhruv, “Issue #5 - visualnav transformer,” GitHub Issues, 2025, accessed: 2025-03-01. [Online]. Available: <https://github.com/robodhruv/visualnav-transformer/issues/5>
- [38] A. Eftekhar, L. Weihs, R. Hendrix, E. Caglar, J. Salvador, A. Herasti, W. Han, E. VanderBil, A. Kembhavi, A. Farhadi, *et al.*, “The One RING: a Robotic Indoor Navigation Generalist,” *arXiv preprint arXiv:2412.14401*, 2024.
- [39] S. Umeyama, “Least-squares estimation of transformation parameters between two point patterns,” *IEEE Transactions on Pattern Analysis & Machine Intelligence*, vol. 13, no. 04, pp. 376–380, 1991.
- [40] K. Zakka, B. Tabanpour, Q. Liao, M. Haiderbhai, S. Holt, J. Y. Luo, A. Allshire, E. Frey, K. Sreenath, L. A. Kahrs, *et al.*, “Mujoco playground,” *arXiv preprint arXiv:2502.08844*, 2025.